PROCEEDINGS OF SCIENCE

Hardware Overview for the Radio Neutrino Observatory in Greenland

Ryan Krebs[a,*] **on behalf of the RNO-G collaboration**

[a] *Dept. of Physics, Pennsylvania State University,*
251 Pollock Road, State College, PA, US

E-mail: rjk5416@psu.edu

The Radio Neutrino Observatory in Greenland (RNO-G) is an under-construction ultra-high energy neutrino detector (>10PeV) that is composed of independent, autonomous, and low power stations featuring their own power, data acquisition, and communications systems. At the beginning of the summer of 2024, we have deployed 7 of 35 stations. The stations have been collecting data for the past three years. We present a broad overview of the current hardware and further show recent and upcoming upgrades to the DAQ and trigger firmware. These upgrades will improve operations, neutrino sensitives, and our ability to discriminate against cosmic ray background signals in future studies. Additionally, we present updates on supplementing power to the solar power with wind turbines that can help extend season livetime into the winter months.

10th International Workshop on Acoustic and Radio EeV Neutrino Detection Activities (ARENA2024)
11-14 June 2024
The Kavli Institute for Cosmological Physics, Chicago, IL, USA

*Speaker

PoS(ARENA2024)002

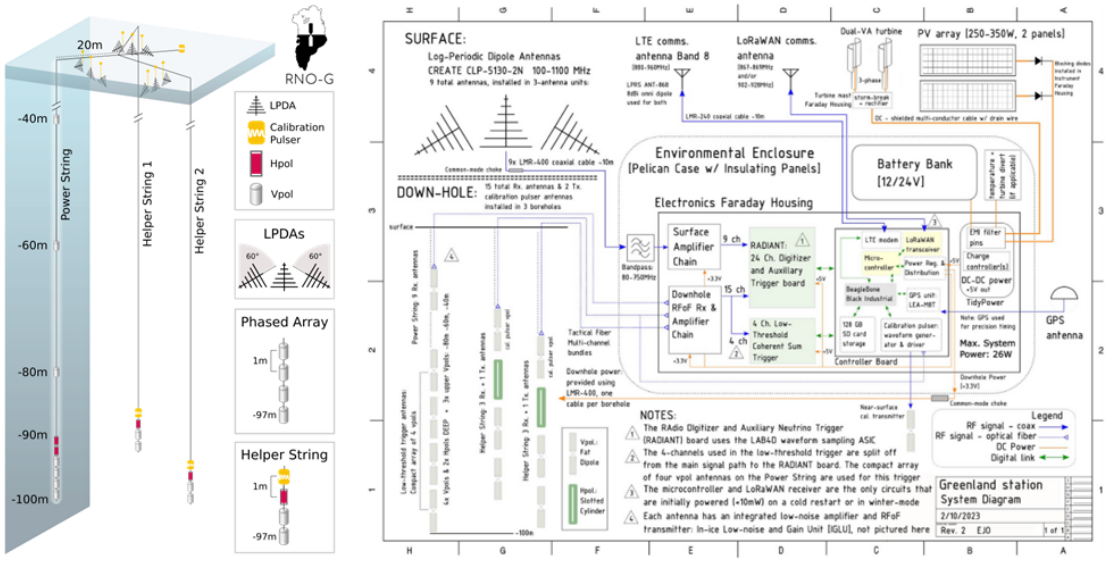

Figure 1: Left: Antenna layout of a typical RNO-G station. Right: System diagram for a typical RNO-G station.

1. Introduction

The Radio Neutrino Observatory in Greenland (RNO-G) is an upcoming neutrino detector aiming to discover the first ultra-high enegry (UHE) neutrinos by using the radio pulses generated from the Askaryan effect of particle showers in ice. The detector builds upon techniques and designs of other in-ice based experiments of ARA [1, 2] and ARIANNA [3]. RNO-G is composed of independent, autonomous stations each capable of triggering and recording data. Each station is outfitted with in-ice and near surface antennas, low power RF chain, data acquisition, triggering, station control, low-power communications over LoraWAN, higher throughput communication over LTE, and a suite of renewable energy sources. Figure 1 details each station's design and shows the full system diagram. Further details of the experiment can be found in the design paper [4] and [5, 6].

The radio frequency (RF) system design is different for the surface and deep components. The deep component is composed of vertically polarized (Vpol) antennas, horizontally polarized (Hpol) antennas, low-noise and low-power amplifiers, filters, cabling using RF over fiber (RFoF) and coaxial cables, a dedicated trigger board, and digitizer board. The Vpol and Hpol antennas are deployed into boreholes. Signals from these antennas are amplified and transmitted via optical using RFoF in the In-Ice Gain and Low Power Unit (IGLU). Upon arriving at the surface, signals are converted back to electrical, amplified, and filtered for a second stage with the Downhole Receiver and Amplifier Board (DRAB). The four lowest Vpol antennas named the Phased Array are split between the digitizer, **Ra**dio **Di**gitizer and **A**uxillary **N**eutrino **T**rigger (RADIANT), and to the dedicated trigger board, **Fl**exible **O**ctal **W**av**e**form **R**ecorder (FLOWER). The other channels exclusively go to the RADIANT. The surface component is composed of log period dipole antennas (LPDAs), coaxial cables, low noise amplifiers and filters, and the RADIANT. From the deployment

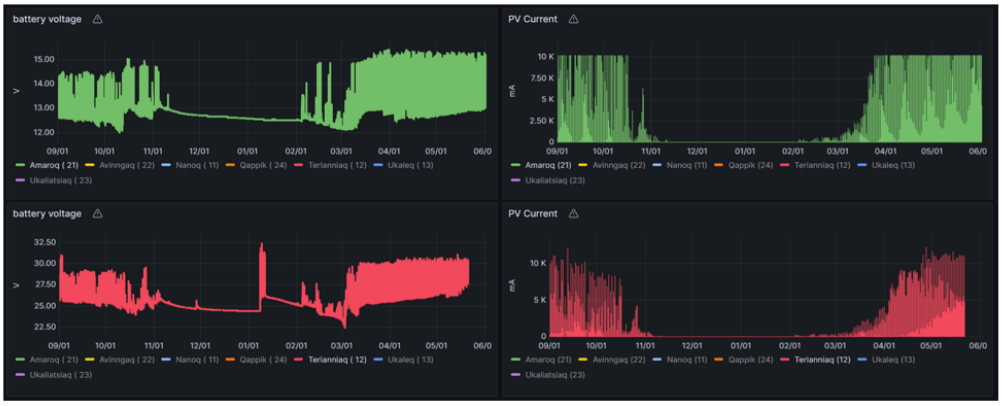

Figure 2: Readout from monitoring tools for a yearly power draw comparison of station 21 with (top, green) and station 12 without (bottom, red) wind turbines. With zero PV current during the winter months, the battery voltage of station 12 shows charging during the winter where no sun is present.

of our first station in 2021 to this year's deployment, we've made notable improvements to the power system, RF chains, trigger, and digitizer firmware.

2. Power System

Each station is autonomous and independent, meaning that it relies on its own supply of power and continuously collects data without interruption. The power draw for a full station in data-collection mode is ~28W. Power usage can be broken down as follows: the RADIANT uses ~12W, the FLOWER uses ~3W, the amplifiers use ~6W, and the remaining housekeeping and computing take up ~7W. Until 2022, stations only relied on two 120W solar panels. This sufficiently powers the stations for ~50% livetime. While the sun is above the horizon we safely shut down data collection early enough to not deplete battery. This presents a significant hit to our sensitives by limiting how long during the year we can run. Therefore we explore supplementing the solar power with wind power, which is reliably present all year.

At an elevation of ~3200m above sea level, Summit Station experiences year-round wind. To harness this power we are exploring small scale off-the-shelf turbines with the target of supplying >~30W on average. In 2022, station 11 and station 12 were outfitted with two vertical/cylindrical wind turbines each as seen in Figure 3. The total livetime accumulated by station 11 in the 2023 data collection season is higher than non-wind power stations (13, 23, 24) by ~5-15% (7-25 days). Figure 2 compares the battery charge and PV current in station 21, without wind turbines, and station 11, with wind turbines using our monitoring tools. The turbines increased the livetime and has shown to be able to charge the stations during winter. The disadvantage of the cylindrical turbines were susceptible to accumulating snowdrift and freezing stuck. For the 2024 deployment season we will be outfitting each station with a different design of wind turbine and will transition the power system to be contained in an external power box that accepts solar and wind inputs without extra modification. The box will also ease station maintenance as snow drift covers the environmental box.

Figure 3: Left: 2022-2024 Prototype wind turbine. Right: Station 11 surface.

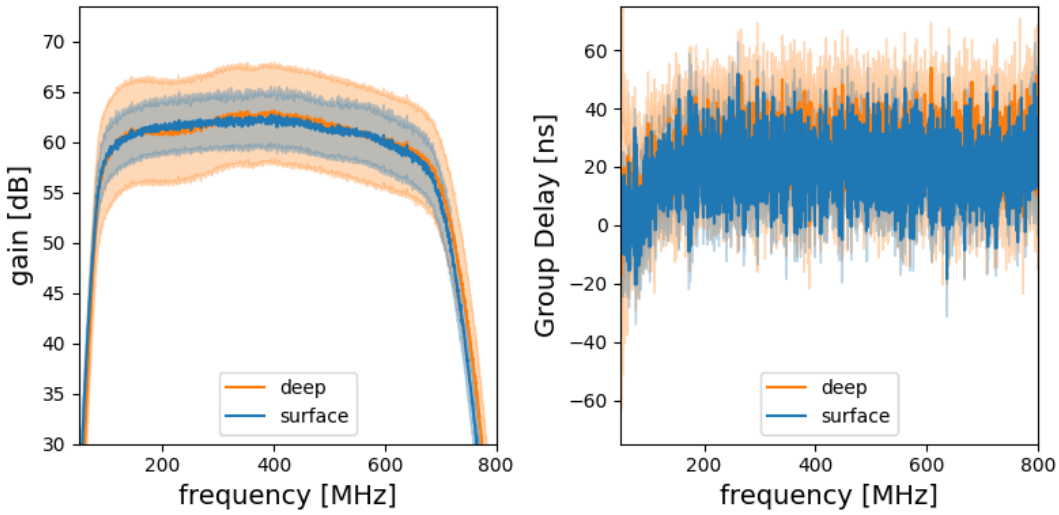

Figure 4: Gain and group delays of chosen components for deep and surface RF chains for upcoming stations.

3. RF System

The RF system is composed of deep and surface channels to capture frequencies contained in Askaryan pulses. The deep antennas, fat dipole antennas and quadslot antennas, are geometrically constrained to fit into boreholes. These have been discussed in [5, 7, 8]. The amplifiers feature low-pass and high pass-filters with low noise amplifiers to target ~80-800MHz bandwidth with ~60dB of total gain across the band. These have been extensively discussed in [5, 9]. The gain and group delays of deep and surface chains can be seen in Figure 4. Each deep channel consumed ~0.24W and each surface channel uses ~0.23W to bring the total power to ~6W.

The RADIANT digitizer board is made of 24 LAB4D sampling chips [10], a "boardmanager" microcontroller, and two CPLDs to breakout to the larger Artix 7 FPGA. It is configured to run 2048 sample buffer lengths and at 3.2 GHz during the 2021-2023 data. It can use a diode-based integrated power coincidence trigger on any combination of channels. Two of these triggers are in use, the first is the upward-facing surface trigger which looks for a 2 of 3 coincidence on the

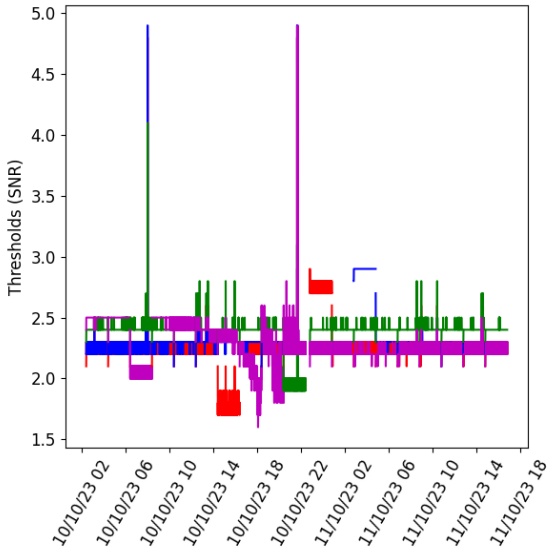

Figure 5: Thresholds for the low-threshold coincidence trigger on the phased array channels during a normal period on station 23. The discreteness of the thresholds, in SNR on an assumed V_{RMS} = 5 ADC, are due to the integer thresholds in ADC.

upward pointing LPDAs, the second is a downward-facing surface trigger with looks for a 4 of 6 coincidence on the downward pointing LPDAs. The upward trigger is the "cosmic ray veto" trigger and the downward trigger is used to supplement the low-threshold trigger.

The FLOWER board is the designated low-threshold trigger board that runs on the lowest 4 Vpol antennas on the "power string" (aka the phased array). It uses two HMCAD 1511 streaming digitizer chips, configured with 2 channel inputs each at a sampling rate of 472 MHz. The lower bandwidth optimizes the trigger efficiencies as described in [11]. The RF frontend is made of an anti-aliasing (high-pass) filter at 250MHz. The gains of each channel are set so that each channel has a V_{RMS} > 5 ADC. Digitized signals in the sampling chips are fed to the Cyclone V FPGA over SERDES in 4 sample blocks. It has been running a 2 of 4 high-low threshold coincidence trigger in a window of 12 ns for high-low coincidence and 42 ns for coincidence between channels. When the coincidence criteria is satisfied, the trigger signal is passed from the FLOWER to the RADIANT for readout of all 24 channels. Figure 5 shows the coincidence trigger thresholds over time in units of SNR as defined with $V_{pk-pk}/(2 * V_{RMS})$ on an assumed V_{RMS} = 5 ADC.

3.1 DAQ Firmware for Cosmic Rays

Cosmic rays (CR) are not uncommomn in RNO-G and are a known background that can have signal penetrate the ice and appear in the deep channels as neutrino-like. To better detect CR and discriminate to neutrinos, we use the upward-facing RADIANT trigger to identify signals coming from above. Thoguh due to the geometry and the simultaneous readout of all channels in the DAQ, physical signals coming from the deep channels are not captured in the readout window. Figure 6 illustrates the propagation delays compared to trigger times. In order to better acquire the CR background [12] in the deep channels we need to increase the buffer length and/or readout the channels at different times. For these reasons, the sampling rate was changed from 3.2 GSps to 2.4

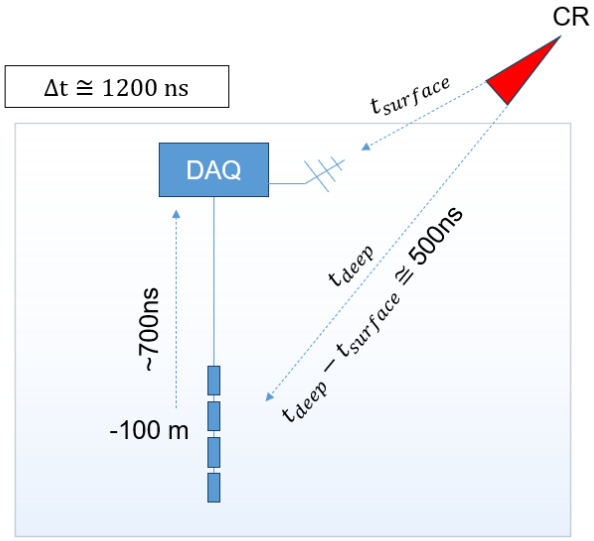

Figure 6: Diagram showing the needed readout delays when a cosmic ray triggers the surface channels and propagates to the deep channels.

GSps. Then we added FPGA firmware to apply different readout delays to specific channels based on trigger type. For the upward-looking triggers, we apply a readout delay to the deep channels of ~1100 ns to counter the ice propagation and the different cables delay times between surface and deep channels [12]. For the downward-looking triggers we can apply ~300 ns delays to the deep channels as the cable delays and ice propagation direction are smaller. This firmware has been deployed starting in the 2024 data collection season. By using these delays we expect to see cosmic rays clearly identifiable in both the surface and deep channels. This will better inform comic ray and neutrino searches.

3.2 Trigger Firmware

The current trigger running on the FLOWER is a high-low voltage threshold trigger. This trigger design is suboptimal to the designed beamformed/phased array trigger in [4] which uses coherence between physical signals to better improve voltage SNRs by $\sqrt{N_{ant}}$. It derives from the ARA-5 Phased Array [2]. A new beamformed trigger is in developement. This trigger works by delaying and summing the four phased array channels together based on signal arrival times using a plane wave approximation and calibrated cable delays. A power integration trigger is applied to the coherently summed waveform. Eight beams are located at elevation angles of -60°,-42°,-25°,-9°,9°,25°,42°,60°.

Due to the closeness of the phasing antennas and the low sampling rate, beamforming is not so trivial. The coherently summed waveform has to be done on an upsampled version of the signal. The best upsampling method using FFT zero packing is unrealizable on such a small, and fast paced, FPGA design. For now, 4x linear interpolation is applied. More advanced upsampling methods using CIC filters or FIR filters are being tested. Figure [11] shows the lab measured trigger efficiency on a perfectly coherent signal. Even with a simple upsampling method, the phased trigger

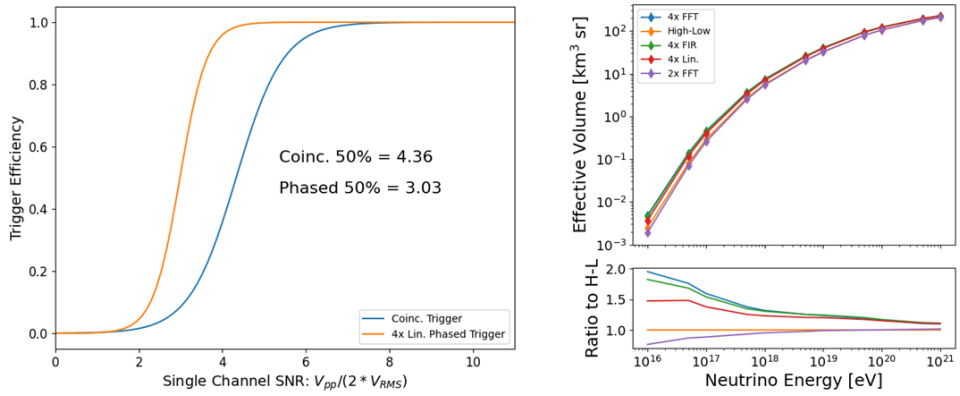

Figure 7: Left: Lab-measured trigger efficiency for the current coincidence trigger and in-development linearly interpolated phased trigger using a pulse generator and noise from the real signal chain. Right: Simulated effective volumes of an RNO-G station using various upsampling factors and methods to ν_e neutral current interactions.

improves upon the high-low threshold trigger. Simulations using NuRadioMC [13], with only ν_e neutral current (NC) interactions as a representative set show that the upsampling is necessary and the implemented method needs to approach an ideal FFT upsampling as seen in Figure 7.

4. Conclusion

RNO-G has had operating stations since 2021. These stations have shown the low-power design running on solar energy is capable to run continuously for half the year. Prototyping wind turbines on a few stations has improved their livetime by extending data collection further into the winter and gives promise for a boost in sensitivities by outfitting all stations with turbines. The data collected uses low thresholds that will only be improved upon with a new beamformed trigger. Furthermore, the ability to identify cosmic rays has been improved by implementing new firmware that allows for all channels to contain cosmic ray signals. These improvements will impact future cosmic ray and neutrino detection by increasing sensitivies across all energies and by better discriminating backgrounds.

References

[1] P. Allison, J. Auffenberg, R. Bard, J.J. Beatty, D.Z. Besson, S. Boeser et al., *Design and initial performance of the askaryan radio array prototype eev neutrino detector at the south pole*, 2011.

[2] P. Allison, S. Archambault, R. Bard, J. Beatty, M. Beheler-Amass, D. Besson et al., *Design and performance of an interferometric trigger array for radio detection of high-energy neutrinos*, *Nuclear Instruments and Methods in Physics Research Section A: Accelerators, Spectrometers, Detectors and Associated Equipment* **930** (2019) 112–125.

[3] L. Gerhardt, S. Klein, T. Stezelberger, S. Barwick, K. Dookayka, J. Hanson et al., *A prototype station for arianna: A detector for cosmic neutrinos*, *Nuclear Instruments and Methods in Physics Research Section A: Accelerators, Spectrometers, Detectors and Associated Equipment* **624** (2010) 85–91.

[4] J. Aguilar, P. Allison, J. Beatty, H. Bernhoff, D. Besson, N. Bingefors et al., *Design and sensitivity of the radio neutrino observatory in greenland (rno-g)*, *Journal of Instrumentation* **16** (2021) P03025.

[5] D. Smith, *Topics on the Detection of Ultra-High Energy Neutrinos*, Ph.D. thesis, The University of Chicago, 2022.

[6] L. Pyras, *Cosmic Rays and the Radio Neutrino Observatory Greenland (RNO-G)*, Ph.D. thesis, Friedrich-Alexander-Universität Erlangen-Nürnberg, 2024.

[7] RNO-G collaboration, *Hardware Development for the Radio Neutrino Observatory in Greenland (RNO-G)*, *PoS* **ICRC2021** (2021) 1058.

[8] RNO-G collaboration, *Performance of the Horizontally Polarized Antennas Used in the Radio Neutrino Observatory in Greenland*, *PoS* **ICRC2023** (2023) 1133.

[9] RNO-G collaboration, *Low-Power Radiofrequency Systems for the RNO-G Project*, *PoS* **ICRC2023** (2023) 1171.

[10] J.M. Roberts, G.S. Varner, P. Allison, B. Fox, E. Oberla, B. Rotter et al., *Lab4d: A low power, multi-gsa/s, transient digitizer with sampling timebase trimming capabilities*, *Nuclear Instruments and Methods in Physics Research Section A: Accelerators, Spectrometers, Detectors and Associated Equipment* **925** (2019) 92–100.

[11] C. Glaser and S. Barwick, *An improved trigger for askaryan radio detectors*, *Journal of Instrumentation* **16** (2021) T05001.

[12] L. Pyras, C. Glaser, S. Hallmann and A. Nelles, *Atmospheric muons at pev energies in radio neutrino detectors*, *Journal of Cosmology and Astroparticle Physics* **2023** (2023) 043.

[13] C. Glaser, D. García-Fernández, A. Nelles, J. Alvarez-Muñiz, S.W. Barwick, D.Z. Besson et al., *Nuradiomc: simulating the radio emission of neutrinos from interaction to detector*, *The European Physical Journal C* **80** (2020) .